



Preparation of Fe₃O₄/organo-montmorillonite nanocomposite and its use as an adsorbent for removal of an anionic dye

Özkan Açışlı

Ataturk University, Faculty of Earth Sciences, Department of Petroleum and Natural Gas Engineering, 25400, Oltu, Erzurum, Turkey, Tel. +90 442 816 4478-5940, Fax +90 442 816 4479, email: ozkan.acisli@atauni.edu.tr (Ö. Açışlı)

Received 3 April 2018; Accepted 29 October 2018

ABSTRACT

In the present study, the adsorption process was employed for removal of Reactive Yellow 81 (RY81) from aqueous solutions using a magnetically separable Fe₃O₄/Organo-montmorillonite (OMt) nanocomposite as an adsorbent. The synthesized material, which is composed of Fe₃O₄, dodecyl trimethyl ammonium bromide (DTAB) and montmorillonite (Mt), was characterized by X-ray diffraction (XRD), scanning electron microscopy (SEM) and Fourier transform infrared spectroscopy (FTIR) analyses. Characterization results confirmed the well integration and incorporation of Fe₃O₄ nanoparticles and DTAB molecules into the Mt clay galleries. The removal efficiency of RY81 was examined at 20°C, and studied as a function of adsorbent amount (0.5–2.0 g/L), initial dye concentration (20–100 mg/L), initial pH (2–11) and contact time (0–60 min). According to the experimental results, the removal efficiency decreased with the increasing initial dye concentration and pH. Besides, the optimum adsorbent dosage was determined as 1.25 g/L. The removal efficiency of 84.29% was achieved with the adsorbent dosage of 1.25 g/L, the initial dye concentration of 20 mg/L, the residence time of 60 min and the pH of 7.40. Experimental data were analyzed using different equilibrium isotherms such as Langmuir, Freundlich, Temkin, BET, Dubinin-Radushkevich and Harkins-Jura isotherms. The analysis results indicated that the adsorption process fitted well to pseudo-second-order, intra-particle diffusion kinetics and the Langmuir model. In addition, the adsorption occurs through the physical interactions and increases the adsorbed amount of anionic dye molecules by increasing the partial positive surface charge. Overall results have suggested that the Fe₃O₄/OMt can be used as a promising adsorbent in adsorption process for the applications of dye removal from aqueous solutions.

Keywords: Magnetite nanoparticles; Reactive Yellow 81; Textile dye; Wastewater treatment

1. Introduction

The various kinds of synthetic dye and pigments released from various industries such as paper, textile, plastic, leather and food are the main organic pollutant compounds in wastewater [1,2]. The presence of these dyes has detrimental effects on humans and environment because of their carcinogenic and toxic content [3]. Therefore, discharging of these effluents into the receiving body without any treatment is really important in terms of the environmental point of view [1,4]. The anionic Reactive Yellow 81

(RY81) dye used in this study is very stable to sunlight, and has a considerable resistance to biodegradation and natural oxidizing agents [5].

Various chemical and physical methods such as ozonation, adsorption, advanced oxidation processes, coagulation/flocculation, membrane filtration and biological treatment techniques are used to reduce hazardous pollutants present in the effluents [6–10]. Among these methods, the adsorption process has attracted great interest due to its simplicity, high efficiency and low cost [11,12]. Especially activated carbon, an effective adsorbent for the removal of dissolved organic substances, is widely used in the adsorption studies. However, the use of activated carbon

*Corresponding author.

is restricted due to its high processing costs and the limitations in its applications [13,14]. To overcome these disadvantageous situations related to the activated carbon usage, new and cheaper alternative adsorbents have been studied by many researchers [14]. Clay is one of the alternative adsorbents for the mentioned applications due to its low cost, abundance, mechanical and chemical stability, non-toxic and environmentally friendly nature [15].

The pristine clay can play an important role in eliminating neutral organic contaminants due to the low charge density on its surface [16]. However, pure clay is not effective enough to remove some anionic contaminants from aqueous solutions. Therefore, it should be modified with proper chemicals for the effective removal of negatively charged contaminants. The most widely used method for this purpose is the ion exchange where inorganic cations in the interlayer galleries of clay are commonly replaced by organic cations of quaternary ammonium salts [14,15]. In addition, impregnation of a super-paramagnetic nanoparticle, such as Fe_3O_4 , with montmorillonite clay has been recently used for the removal of contaminants since the resultant nanocomposite does not need to be centrifuged or filtered. Nowadays, the usage of magnetic adsorbents to deal with environmental issues is of great interest because the magnetic adsorbents can be easily separated from the area by a simple magnet after the adsorption process [17].

In this work, a nanocomposite material was first synthesized from magnetic Fe_3O_4 nanoparticles, cationic dodecyl trimethyl ammonium bromide (DTAB) surfactant and negatively charged montmorillonite (Mt) under sonication. The obtained super-paramagnetic Fe_3O_4 /Organo-montmorillonite (OMt) nanocomposite was then used as the adsorbent to effectively remove Reactive Yellow 81 (RY81) as a model pollutant from aqueous solutions. The selection of this anionic dye is due to its great importance in water treatment. The experimental variables, namely adsorbent amount, initial dye concentration, contact time and pH were selected to evaluate the removal efficiency. In order to better explain the adsorption mechanism, the kinetic and equilibrium studies of removal RY81 with Fe_3O_4 /OMt were also accomplished. To sum up, the aim of this study was to prepare a nanocomposite and use it as an adsorbent for removal of an anionic dye.

2. Experimental

2.1. Materials

K10 Montmorillonite (Mt) used in the study was purchased from Sigma-Aldrich Co. (USA). It has a surface area of $279.28 \text{ m}^2/\text{g}$, and consists of SiO_2 , Al_2O_3 , Fe_2O_3 , MgO , CaO , Na_2O , and K_2O with 66.9, 13.8, 2.8, 1.6, 0.3, 0.2 and 1.7% by weight, respectively. The cation-exchange capacity (CEC) of the Mt sample, which is $120 \text{ meq}/100 \text{ g}$, was determined by the ammonium acetate method. In this method, a certain amount of Mt sample was first mixed with the $10 \text{ ml } 0.1 \text{ M}$ ammonium acetate solution. The suspension was then subjected to ultrasonic bath treatment for 24 h. After that, the supernatant was removed by centrifugation, and a new salt solution was obtained. 10 ml of distilled water was then added to remove excess salt from the clay suspension. All of the supernatant fractions collected for each treatment

were combined to have a considerable volume, and then analyzed for their metallic cations by atomic absorption spectroscopy. The CEC of the Mt was eventually calculated from the division of the measured cations' quantities by the mass of the dried Mt sample [15,18,19].

The analytical grade anionic RY81 dye was bought from Haining Deer Chemical Co. (China), and used without any further treatment. The chemicals used for the synthesis of magnetic Fe_3O_4 were $\text{FeCl}_3 \cdot 6\text{H}_2\text{O}$, $\text{FeSO}_4 \cdot 7\text{H}_2\text{O}$ and dodecyl trimethyl ammonium bromide (DTAB). They were all analytical grade and purchased from Sigma Aldrich Co. All of the other chemicals and reagents used were also analytical grade, and they were provided from Merck (Germany). Distilled water was used throughout the experiments. The structure and properties of the RY81 and DTAB are illustrated in 1.

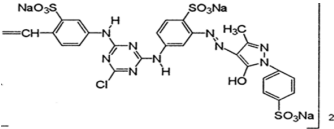
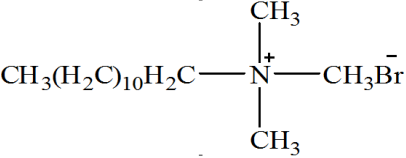
2.2. Preparation of magnetic Fe_3O_4 /OMt nanocomposite

Firstly, 1 g of the K10 Mt was dispersed in 100 mL distilled water and stirred at 250 rpm for 24 h using a thermostatic shaker at the constant temperature of 20°C . Then, an aqueous dispersion was formed, in which Na montmorillonite was expanded by swelling and reached homogeneity. Meanwhile, 1.050 g $\text{FeCl}_3 \cdot 6\text{H}_2\text{O}$ and 0.600 g $\text{FeSO}_4 \cdot 7\text{H}_2\text{O}$ were added into 50 mL distilled water, and the ratio of ferrous to ferric ions in the solution was adjusted to $1.0/1.8$ by this way. After that, 10 mL NH_3 solution (8M) was added drop by drop to generate magnetic iron oxide under N_2 atmosphere [20]. In order to examine the effect of Fe_3O_4 amount in composite material, 0.5 gram of the synthesized Fe_3O_4 nanoparticles ($\text{Mt}/\text{Fe}_3\text{O}_4 = 1/2$) were separately added to the DTAB solution (1.0 CEC of Mt), and then continuously sonicated for 8 h to produce monodispersed Fe_3O_4 . At the end of the sonication, nano-crystalline particles stabilized by DTAB were eventually formed [21]. The obtained nanoparticles was then mixed with the previously prepared K10 montmorillonite suspension, and stirred slowly for 24 h . Greyish black precipitates were finally obtained, and washed with distilled water and ethanol successively for several times to remove the residual ions. The resultant obtained magnetic Fe_3O_4 /OMt nanocomposite was then dried in vacuum at room temperature, and finally stored in a closed vessel until its use in the experiments. In order to emphasize the higher adsorption efficiency of the new Fe_3O_4 /OMt adsorbent, the experiments were also carried out using DTAB/Mt adsorbent under the same conditions. This time organo-clay sample was prepared by adding DTAB solution (1 CEC of Mt) into aqueous suspension of 1 g K10 Mt.

2.3. Characterization of magnetic Fe_3O_4 /OMt nanocomposite

The crystalline structure of as-prepared samples was examined via XRD analysis with $\text{Cu-K}\alpha$ radiation (40 kV , 30 mA , 1.54051 \AA) over a 2θ range from 5° to 70° at room temperature (PANalytical Empyrean X-Ray Diffractometer, USA). The surface morphologies of magnetic Fe_3O_4 /OMt nanocomposites were observed using a high-resolution scanning electron microscope (SEM). Fourier transform infrared (FTIR) spectra were recorded on a Tensor 27, Bruker (Germany), in a wavenumber range of $4000\text{--}400 \text{ cm}^{-1}$ by using the KBr pellet technique.

Table 1
Chemical structure and characteristics of RY81 and DTAB

C.I. name	Chemical structure	Chemical structure	M_w (g mol ⁻¹)	λ_{max} (nm)	CMC (mol/L)
Reactive yellow 81	C ₃₂ H ₃₄ C ₁₂ N ₁₈ Na ₆ O ₂₀ S ₆		1632.18	394	
DTAB	CH ₃ (CH ₂) ₁₁ N(CH ₃) ₃ Br			308.34	15.10 10 ⁻³ (4810 mg/L)

The pH of zero point charge (pH_{zpc}) for the magnetic Fe₃O₄/OMt nanocomposite sample was determined based on the method suggested by Bessekhoud et al. [22]. According to this method, 100 mL of 0.01 M NaCl solution was prepared, and transferred into conical flasks, in which the pH values were adjusted in the ranges of 2–11 using HCl and NaOH solution. 0.1 g of the magnetic Fe₃O₄/OMt nanocomposite sample was added to each flask, and the suspension was then stirred in a shaker for 48 h. The final pH values of each solution were measured, and the differences between the initial and final pH values (ΔpH) were determined. The ΔpH values were plotted against the initial pH values. Finally, the point where ΔpH is equal to zero was determined as pH_{zpc}.

2.4. Batch adsorption experiments

In order to investigate the adsorption capacity of the magnetic Fe₃O₄/OMt nanocomposite, the effects of the experimental parameters, namely adsorbent dosage, initial RY81 concentration, pH and adsorption time were studied. Batch adsorption experiments were performed in 150 ml glass-stoppered, round-bottom flasks immersed in a temperature controlled thermostatic shaker at constant stirring rate (120 rpm) and temperature (20°C) in neutral pH of 7.40. According to the preliminary experiments, all of the adsorption tests were carried out using the predetermined optimum conditions, which are 0.125 g magnetic Fe₃O₄/OMt nanocomposite and initial dye concentration of 20 mg/L. At certain time intervals, the magnetic Fe₃O₄/OMt adsorbent was separated, and a pre-determined amount of sample was then taken from the solution by means of a permanent hand-held magnet and a single channel adjustable pipette. RY81 concentration in the solution was determined using a UV-Vis spectrophotometer (Optizen pop, Korea) at 394 nm (λ_{max} for RY81). The adsorbed amount at equilibrium (q_e) and a specific time (q_t), and the removal efficiency (RE, %) of RY81 were calculated using the following equations:

$$q_e = \frac{(C_0 - C_e)V}{W} \tag{1}$$

$$q_t = \frac{(C_0 - C_t)V}{W} \tag{2}$$

$$RE(\%) = \frac{(C_0 - C_e)}{C_0} \times 100 \tag{3}$$

where q is RY81 uptake (mg/g), C₀ is initial concentration of dye (mg/L), C_e is equilibrium concentration of dye (mg/L), V is the volume of solution (L), and W is the dry weight of the added adsorbent (g). To obtain the adsorption isotherms of RY81, varying initial dye concentrations were run with the same procedure as described above at room temperature (20°C).

The point of the maximum absorbance wavelength for RY81 was determined using different dye concentrations. As seen from Fig. 1, the maximum absorbance wavelength (λ_{max}) was found as 394 nm.

3. Results and discussion

3.1. Structural analysis of magnetic Fe₃O₄/OMt nanocomposite

The XRD patterns of magnetic Fe₃O₄/OMt nanocomposite are shown in Fig. 2. The components of raw material are mainly composed of montmorillonite (JCPDS file no. 29-1498) and quartz (JCPDS file no.46-1045) [16]. From the XRD pattern of the magnetic Fe₃O₄ nanoparticle, the diffraction peaks at 2θ value of 17.90°, 29.50°, 35.40°, 43.05°, 53.40°, 56.90 and 62.40° were completely matched the reflections of (111), (220), (311), (400), (422), (511) and (440) respectively. All the observed Fe₃O₄ peaks in the structure can be indexed as the cubic phase of Fe₃O₄ (JCPDS No. 19-0629) [23–25].

The 2θ value of the d001 peak of the montmorillonite has 8.90° and the corresponding basal spacing is 0.99 nm. This value is suited with a basal spacing of natural montmorillonite. The 2θ value of the d001 peak is shifted from 8.90° towards to 7.70° after modification with only DTAB and basal spacing of the OMT was 1.14 nm. This value is compatible with the work of Açıslı et al. [26]. The incorporation of Fe₃O₄ nanoparticles and DTAB molecules into the Mt clay galleries increased the d001-value from 1.14 nm to 1.28 nm. It is indicated that the ferrirous oxide particles may be dispersed both on the external surfaces and the internal surface of Mt spaces, and also displaced during synthesis procedure with DTAB-Fe₃O₄ molecules intercalating into the silicate layers instead of Mg²⁺ and Ca²⁺ metal ions [27].

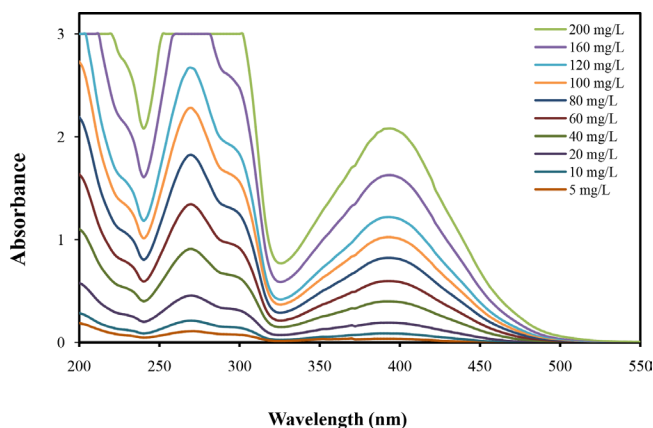


Fig. 1. The maximum wavelength of RY81.

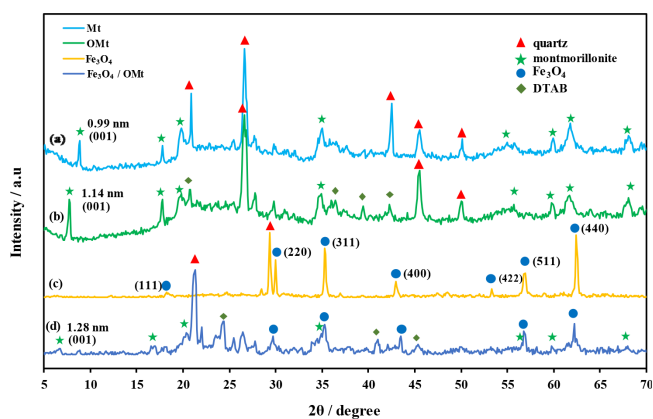


Fig. 2. XRD patterns of (a) Mt, (b) OMt (DTAB/Mt), (c) Fe_3O_4 and (d) $\text{Fe}_3\text{O}_4/\text{OMt}$.

FT-IR spectroscopy was used to confirm the incorporation of Fe_3O_4 and DTAB into interlayer galleries of Mt, and the analysis results can be seen in Fig. 3. According to this figure, the absorption bands at 3620 cm^{-1} is probably as a result of stretching vibrations of absorbed H_2O molecules or structural $-\text{OH}$. A band approximately 1628 cm^{-1} can be due to the $\text{H}-\text{O}-\text{H}$ bending vibration, and attributed to the

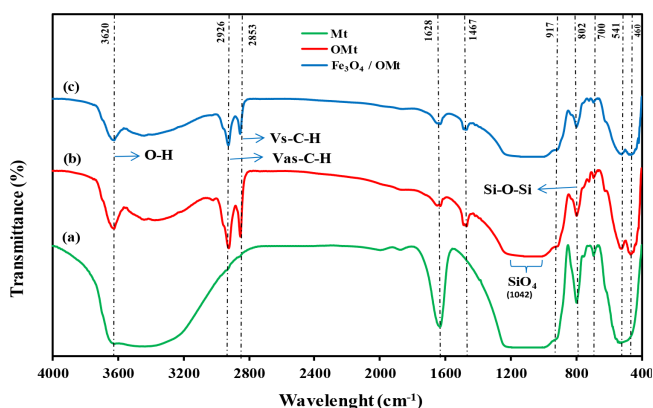


Fig. 3. FTIR spectra of (a) Mt, (b) OMt (DTAB/Mt) and (c) $\text{Fe}_3\text{O}_4/\text{OMt}$.

vibrations of the water molecules [28,29]. The bands at 2926 and 2853 cm^{-1} for all the samples except pure Mt are based on the asymmetric and symmetric stretching vibrations of $\text{C}-\text{H}$ groups. These bands can be attributed to the incorporation of surfactant molecules to the interlayer galleries of Mt [29]. The two absorption bands at 802 and 541 cm^{-1} corresponds to the stretching vibrations of $\text{O}-\text{Si}-\text{O}$ and $\text{Al}-\text{Si}-\text{O}$ groups of the Mt, respectively [28–30]. In addition, the characteristic bands at 573 and 663 cm^{-1} are due to $\text{Fe}-\text{O}$ stretching vibrations [31]. The intensity of the $\text{Si}-\text{O}$ bands in the pure clay is much stronger than that of the magnetic nanocomposite material ($\text{Fe}_3\text{O}_4/\text{OMt}$). It is indicated that the $\text{Fe}-\text{O}$ bonds may have interacted with $\text{Si}-\text{O}$ bonds on the Mt surface during the synthesis [16].

3.2. Morphological analysis

SEM images of the montmorillonite (Mt), organo-montmorillonite (OMt) and $\text{Fe}_3\text{O}_4/\text{OMt}$ nanocomposite samples are given in Fig. 4. As seen from the figure, the Mt sample has some precipitated phase and cracks, and, in general, heterogeneous surface morphology. After the treatment with DTAB, the Mt particles tend to be agglomerated, resulting in a more compact structure. In addition, the cracks and other defects are partly reduced as a result of the modification [29]. From the SEM images of $\text{Fe}_3\text{O}_4/\text{OMt}$ nanocomposite samples, they are very similar to natural magnet, and the magnetic Fe_3O_4 nanoparticles are well dispersed on the surface of Mt without agglomeration. In other words, modification of the Mt by DTAB and magnetic Fe_3O_4 nanoparticles provides an increase in the adsorption capacity.

3.3. Effect of operational parameters on adsorption process

3.3.1. Effect of adsorbent dosage

In order to evaluate the effect of composite nanoparticles dosage on the removal efficiency of RY81, a series of experimental runs were performed using various adsorbent dosage between 0.50 and 2.00 g/L . The obtained results are presented in Fig. 5. As seen from this figure, the reaction reached equilibrium at a specified reaction time of 2.5 min . With increasing adsorbent dosage from 0.5 to 1.25 g/L , the removal efficiency is gradually increased from 31.81 to 84.29% , respectively. The observed improvement in the removal efficiency with the increasing dosage can be attributed to the increase in surface area and availability of more active adsorption sites [15]. However, further increase in the adsorbent dosage beyond 1.25 g/L does not affect the removal efficiency of RY81. Therefore, subsequent experiments were conducted with the composite dosage of 1.25 g/L . Chang et al. studied the adsorption of methylene blue onto $\text{Fe}_3\text{O}_4/\text{activated montmorillonite}$ nanocomposite. They found that color removal increased with the adsorbent dosages of 0.625 to 2.5 g/L , and then remained stable with further increasing [16]. Thus, they determined the optimum dosage as 2.5 g/L and used this value for the rest of the experiments.

3.3.2. Effect of initial RY81 concentration

The effect of initial RY81 concentration on the removal efficiency is shown in Fig. 6. According to this figure, for the

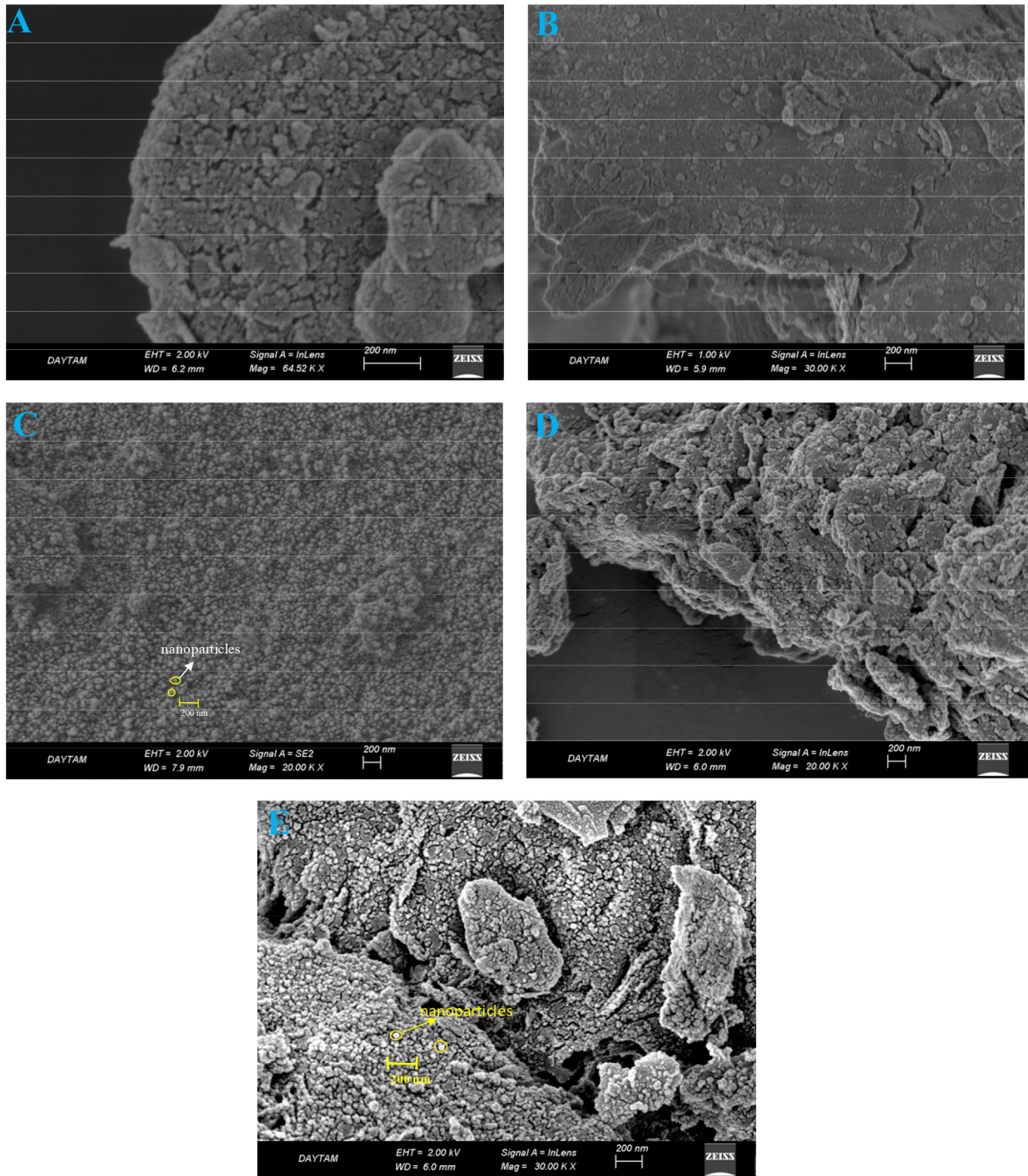


Fig. 4. SEM micro graphs of the samples (a) Mt, (b) OMt (DTAB/Mt), (c) Fe₃O₄ nanoparticles, (d) Fe₃O₄/OMt (Fe₃O₄/OMt = 1/2) and (e) Fe₃O₄/OMt (Fe₃O₄/OMt = 1/4).

residence time of 60 min, the removal efficiency increased from 41.76% to 84.29% by reducing the initial dye concentration from 100 to 20 mg/L. This result can be explained by saturation of the total active adsorption sites at lower dye concentrations [29,32]. Similar results were reported by Chang et al. for the adsorption of methylene blue onto Fe₃O₄/activated montmorillonite nanocomposite [16]. As seen from Fig. 6, the removal efficiency of RY81 initially

increased sharply in the first 2.5 min, and thereafter slowed down since the equilibrium approached. In all the experiments, the interaction time to reach equilibrium was as short as 2.5 min. As known, physical adsorption takes place through physical interactions that do not require any or need a very low activation energy, and it occurs very quickly. On the other hand, a certain activation energy is required for chemical adsorption. The value of this energy is high and a

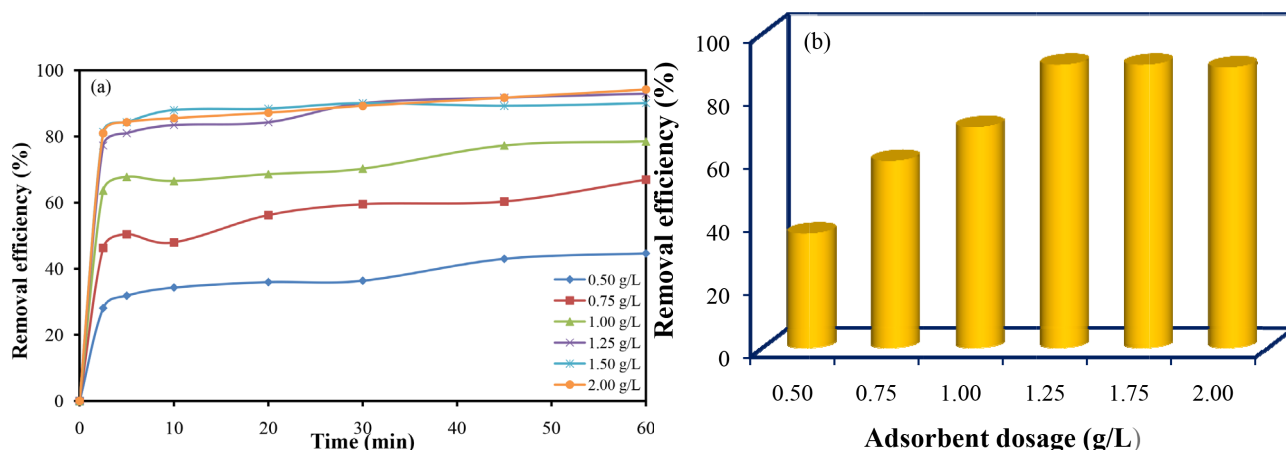


Fig. 5. Effect of adsorbent dosage on the removal efficiency of RY81 a) as a function of time b) for 30 min. Experimental conditions: [RY81]₀: 20 mg/L, Temperature: 20°C, pH: 7.40.

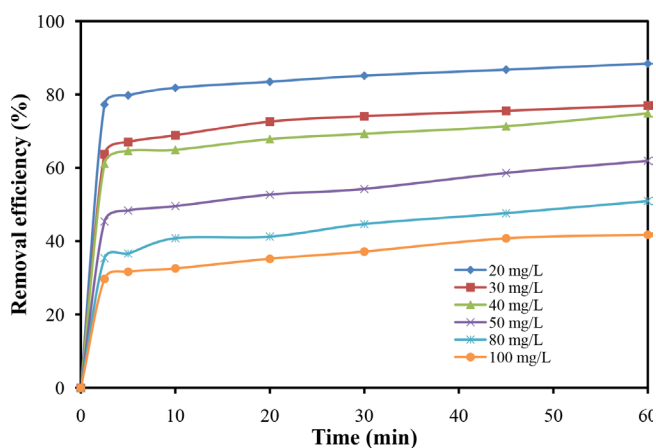


Fig. 6. Effect of initial RY81 concentration on the removal efficiency by adsorption process. Experimental conditions: [Fe₃O₄/OMt]: 1.25 g/L, pH: 7.40, Temperature: 20°C.

certain time is needed to overcome it. Accordingly, the short equilibrium time proves the physical interactions between the adsorbent and RY81 molecules [33,34]. This result is well agreement with the ones from the work of Chang et al. [16].

In adsorption processes, it is generally expected that the more the adsorbent dosage, the shorter the equilibrium time, and similarly, the higher the adsorbate concentration, the longer the equilibrium time. In this study, the first measurements were taken at 2.5 min for the all experiment sets so the equilibrium time was accepted as 2.5 min. However, in reality, it is certainly shorter than or equal to 2.5 min for all of the adsorbent dosages and adsorbate concentrations studied probably due to the more than enough surface active sites for adsorption.

3.3.3. Effect of initial pH

Solution pH is a very important parameter in adsorption studies since it influences surface charge of adsorbent and changes the concentration of the counter ions and the degree of ionization of the adsorbate in solution [35,36]. As seen from Fig. 7, pH has a significant effect on the removal

efficiency of RY81. As pH of the solution increased from 2.0 to 11.0, the removal efficiency substantially decreased from 98.58 down to 20.72%. Since the pH_{zpc} value of the Fe₃O₄/OMt nanocomposite was determined as 7.80, the adsorbent surface is positively charged for pH < 7.8 and negatively charged for pH > 7.8. The high removal efficiencies obtained

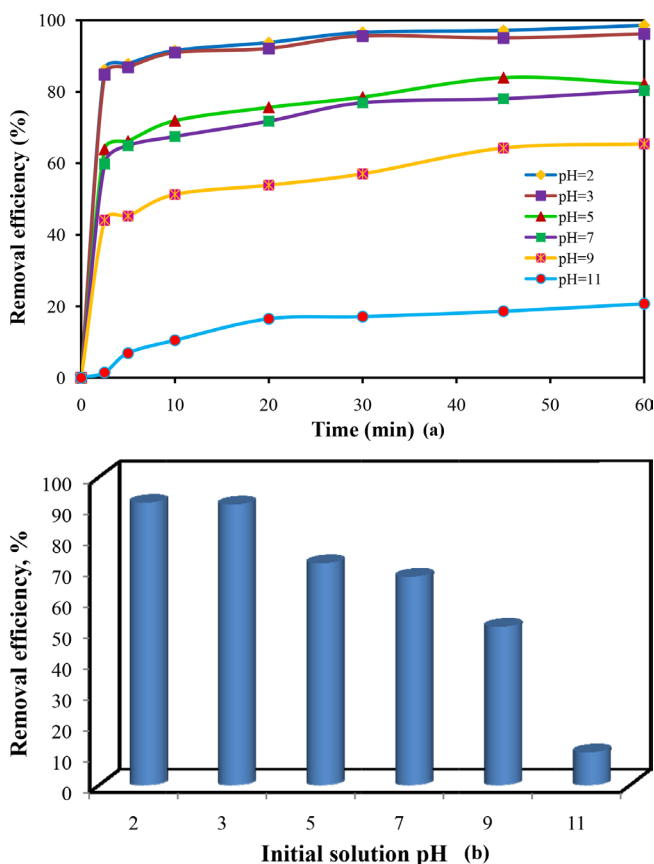


Fig. 7. Effect of pH on the removal efficiency of RY81 during the adsorption process. Experimental conditions: [Fe₃O₄/OMt]: 1.25 g/L, [RY81]₀: 30 mg/L, Temperature: 20°C.

for the pH values of 2 and 3 can be attributed to the high degree of positive charge on the adsorbent surface, which is caused by the protonation at these pH values. As the solution pH increases beyond pHzpc value of the adsorbent, the decrease in removal efficiency of the anionic RY81 can be explained by the increasing negative potential on the surface of the adsorbent, which is resulted from deprotonation. This increasing negative potential leads to the electrostatic repulsion between the adsorbent and the dye molecule, causing a dramatic decrease in the removal efficiency.

In other words, as shown in Fig. 8, when the solution pH is lower than the pHzpc value of the Fe₃O₄/OMt nanocomposite, the degree of positive charge on the adsorbent surface increases due to the increasing [H⁺] at low pH. This results in a significant electrostatic attraction between the anionic RY81 molecules and the adsorbent [29]. On the other hand, at alkaline pH values, the composite surface becomes negatively charged by the excessive [OH⁻], and the electrostatic repulsion occurs between the adsorbent and the RY81 [29,37,38]. In addition, RY81 anionic molecules can compete against OH⁻ ions, and this can reduce their adsorption onto the composite surface [20].

3.3.4. Single effect of the each component

As seen from Fig. 9, the Fe₃O₄/OMt nanocomposite material provided better removal efficiency than the raw Mt

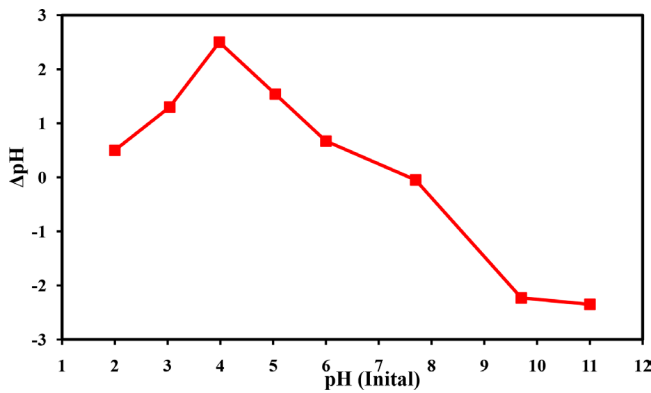


Fig. 8. pHzpc plot of magnetic Fe₃O₄/OMt nanoparticles.

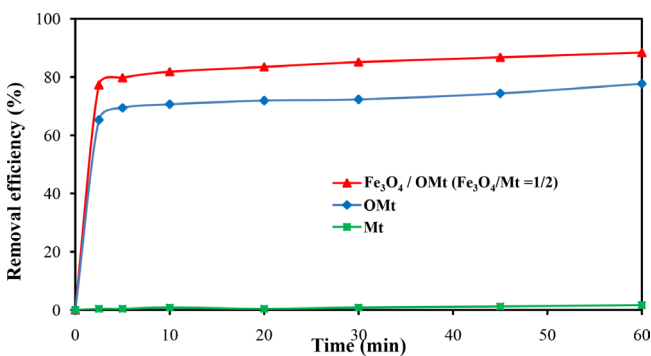


Fig. 9. Effect of enhanced adsorption process. Experimental conditions: [Fe₃O₄/OMt]: 1.25 g/L, [RY81]: 20 mg/L, Temperature: 20°C, pH: 7.40.

and OMt. Due to the negative surface charge of the Mt, the electrostatic repulsion occurs between the dye molecule and the adsorbent, causing a decrease in the removal efficiency. The surface of DTAB modified Mt is positively charged. Therefore, it electro statically attracts the dye molecules, providing an increase in the efficiency of dye removal. In addition, Fe₃O₄ molecules partially cover the clay surface and increase the adsorbed amount of anionic dye molecules by imparting a partial positive charge to the surface [16].

3.3.5. Adsorption kinetics

Three kinetic models including pseudo-first-order, pseudo-second-order and intra-particle diffusion models were used to evaluate the kinetic of RY81 adsorption on the Fe₃O₄/OMt nanocomposite surface. Kinetic studies were carried out with all of the dye concentrations, adsorbent dosage of 1.25 g, temperature of 20°C and pH of 7.40. The equations belonging to these kinetic models are given by Eqs. (4)–(6) [39–44].

$$\ln(q_e - q_t) = \ln q_e - k_1 t \tag{4}$$

$$\frac{t}{q_t} = \frac{1}{k_2 q_e^2} + \frac{t}{q_e} \tag{5}$$

$$q_t = k_i \sqrt{t} + C \tag{6}$$

where q_e and q_t are the amounts of RY81 adsorbed at the equilibrium and a specific time, k_1 (s⁻¹) is the rate constant of the pseudo-first-order model, k_2 is the rate constant (g mg⁻¹ s⁻¹) of the pseudo-second-order model, k_i is the intra-particle diffusion rate constant (mg s^{-1/2} g⁻¹) and C (mg g⁻¹) is the boundary layer thickness [39–41]. The summarized values of the kinetic constants obtained by linear regression analysis are given in Table 2.

The obtained results in this study show that the first order model did not fit, but the pseudo second order model provided high correlation coefficients for all of the dye concentrations ($R^2 > 0.990$). However, the rate constants (k_2) decreased with increasing initial dye concentrations. This result can be attributed to more competition with increasing dye concentration [16,45]. The Weber intra-particle diffusion model is used to describe the steps that take place during the adsorption process. The adsorption process was found to be highly compatible with the intra-particle diffusion model ($R^2 > 0.9600$). The intra-particle diffusion model showed that the thickness of the boundary layer has an effective role in the adsorption process due to the increasing C values with initial dye concentration, indicating a larger boundary layer diffusion effect [16,46,47]. As a result, we can say that the pseudo second-order and the intra-particle diffusion model both occur at the same time. Similar phenomena have been observed for methylene blue adsorption on lignite [45] and onto Fe₃O₄/activated montmorillonite nanocomposite [16].

3.3.6. Adsorption isotherms

Experimental data were applied to the equations of the Langmuir, Freundlich, Temkin, BET, Dubinin-Radushkev-

Table 2
Parameters of the kinetic models used

Initial concentration (mg L ⁻¹)	Temp. °C	Pseudo-first-order		Pseudo-second-order				Intraparticle diffusion		
		k_1	R ²	$k^2 \text{ g mg}^{-1} \text{ s}^{-1}$	$q_{e,exp} \text{ mg g}^{-1}$	$q_{e,cal} \text{ mg g}^{-1}$	R ²	$k_i \text{ 1 mg s}^{-1/2} \text{ g}^{-1}$	C	R ²
20	20	0.0191	0.1669	0.0037	16.6942	16.5289	0.9988	0.0646	13.30	0.9885
30	20	0.0284	0.3371	0.0019	21.7778	23.1481	0.9995	0.0792	19.31	0.9629
40	20	0.0288	0.3003	0.0011	27.1345	29.6736	0.9981	0.1597	22.31	0.9817
50	20	0.0339	0.4217	0.0011	26.3478	30.7692	0.9950	0.1014	24.43	0.9865
80	20	0.0343	0.2827	0.0006	32.9879	40.4858	0.9935	0.2466	27.52	0.9711
100	20	0.0423	0.5385	0.0006	35.1935	42.1941	0.9952	0.2512	28.98	0.9775

ich and Harkins-Jura isotherms to determine the mechanism of the adsorption at 20°C. Isotherm studies were carried out with the adsorbent dosage of 1.25 g, pH of 7.40, and contact time of 2.5 min. The results are given in Table 3, together with the isotherm equations. As seen from Table 3, the regression coefficient of the Langmuir isotherm is higher than those of the other isotherms.

As far as known, Langmuir model assumes that the surface is homogenous and adsorption process is monolayer in nature. But the adsorption may take place via physical interactions, when the pore radius is large enough to allow the adsorbate molecules to attach in a single layer. The

short equilibrium time obtained is the evidence for this. Accordingly, the high R² values obtained for the Langmuir isotherm equation at all initial dye concentrations reveals that this equation describes the process well. This is valid for the mono layer adsorption, and shows that the adsorption occurs due to the very strong electrostatic attractions which the interlayer pores and surface [16,45]. R_L , the dimensionless characteristic of the Langmuir isotherm, is defined by Eq. (7)

$$R_L = \left(\frac{1}{1 + KC_0} \right) \quad (7)$$

Table 3
Applicability of isotherm equations to RY81 adsorption onto Fe₃O₄/OMt surface

Isotherm	Equation	Parameters	Values
Langmuir	$C/q = 1/kq_m + (1/q_m)C$	q_m	32.051
		k	0.148
		R^2	0.9913
		R_L	0.252
Freundlich	$\ln q = \ln k + n \ln C$	n	0.231
		k	11.288
		R^2	0.9155
Temkin	$q_e = (RT/b_T) \ln a_T + (RT/b_T) \ln C_e$	b_T	0.142
		a_T	4.685
		R^2	0.9195
BET	$C/q(1-C) = 1/(q_m k) + [(k-1/q_m k)]C$	q_m	–
		k	0.993
		R^2	0.607
Dubinin-Radukevich	$\ln q = K\epsilon^2 + \ln q_{D-R}$	K	-2×10^{-6}
		q_{D-R}	25.675
		R^2	0.734
Harkins-Jura	$1/q^2 = (B/A) - (1/A) \log C$	B	2.208
		A	416.666
		R^2	0.8654

q , adsorption capacity of RY81 (mg/g); q_m , monolayer adsorption capacity; C , equilibrium concentration; n , k , K , A and B are constant parameters for the isotherm equations.

In which K is the Langmuir constant and C_0 is the initial dye concentration. The obtained R_L values in this study was in the range 0.2522–0.2279 for the $\text{Fe}_3\text{O}_4/\text{OMt}/\text{RY81}$ adsorption system. If the R_L values are $0 < R_L < 1$, this process is favorable for the adsorption.

Freundlich isotherm is a model used to show the interaction between adsorbed molecules in heterogeneous systems. The n parameter represents the heterogeneity factor, and it is used to determine whether the adsorption is a physical ($n > 1$), chemical ($n < 1$) or linear processes ($n = 1$) [45]. According to Table 3, the high R^2 value for $\text{Fe}_3\text{O}_4/\text{OMt}$ nanocomposite shows that the process is suited with the Freundlich isotherm. The n parameter values (0.2313–0.2744) show that the adsorption is favored for the chemical process ($n < 1$), but the interactions between the $\text{Fe}_3\text{O}_4/\text{OMt}$ surface and dye ions are stronger electrostatic attraction. The Temkin isotherm takes into account of the interactions between adsorbent-adsorbate [48]. The heat of adsorption of the all molecules in the layer reduced linearly with coverage layer, and the energy is uniformly distributed [49]. b_T is the constant associated with the heat of adsorption and a_T is the constant related to equilibrium binding constant, corresponding to maximum binding energy.

The obtained values for a_T and b_T are presented together with the value of the correlation coefficient in Table 3. As seen from Table 3, it is better to explain the experimental data ($R^2 > 0.92$) by the Temkin isotherm, which points out that the adsorption of RY81 at 293 K is characterized by a homogeneous distribution binding energies up to the maximum binding energy [45]. The low regression coefficients in BET, Dubinin-Radushkevich and Harkins-Jura isotherms clearly indicate that the adsorption process examined in this study is not compatible with these isotherms.

4. Conclusion

In this study, $\text{Fe}_3\text{O}_4/\text{OMt}$ nanocomposite was used as an adsorbent for the removal efficiency of RY81 from aqueous solutions. The nanocomposite adsorbent was prepared by chemical precipitation with a suitable surfactant under ultrasonic waves. The main findings can be summarized as follows:

- XRD, FTIR and SEM analysis showed that the Fe_3O_4 nanoparticles and DTAB were well intercalated through the clay galleries.
- The equilibrium time for the adsorption process was found as about 2.5 min. The slight change was observed with increasing contact time. This demonstrated that the rapid adsorption occurs mostly through physical interactions.
- The removal efficiency of dye decreased with the increasing initial dye concentration.
- With the increasing adsorbent dosage from 0.5 to 1.25 g/L, the removal efficiency gradually increased from 31.81 up to 84.29%. Further increase in the adsorbent dosage did not affect the efficiency.
- The percentage of color removal decreased with increasing solution pH.
- The pseudo-second-order kinetic model and the intra-particle diffusion model fits very well with

the experimental data of the adsorption of RY81 on the $\text{Fe}_3\text{O}_4/\text{OMt}$ nanocomposite ($R^2 > 0.9900$ and $R^2 > 0.9700$, respectively).

- The regression coefficient obtained for Langmuir isotherm is higher than those for the Freundlich, Temkin, Dubinin-Radushkevich and Harkins-Jura isotherms ($R^2 > 0.9900$). In addition, the monolayer adsorption capacity, $q_{m,r}$ was found as 32.051 mg/g.

In conclusion, overall results have shown that the $\text{Fe}_3\text{O}_4/\text{OMt}$ nanocomposite can be used as an efficient adsorbent for the applications of dye removal from aqueous solutions.

Acknowledgments

Atatürk University Scientific Research Council financially supports this study in the context of a project (Project No: 2015/198), and also the technical support by East Anatolia High Technology Application and Research Center (DAYTAM) from Atatürk University are gratefully acknowledged.

References

- [1] R.D.C. Soltani, A.R. Khataee, M. Safari, S.W. Joo, Preparation of bio-silica/chitosan nanocomposite for adsorption of a textile dye in aqueous solutions, *Intl. Biodeter. Biodegrad.*, 85 (2013) 383–391.
- [2] A. Khataee, M. Sheydaei, A. Hassani, M. Taseidifar, S. Karaca, Sonocatalytic removal of an organic dye using $\text{TiO}_2/\text{montmorillonite}$ nanocomposite, *Ultrason. Sonochem.*, 22 (2015) 404–411.
- [3] C.H. Weng, Y.F. Pan, Adsorption of a cationic dye (methylene blue) onto spent activated clay, *J. Hazard. Mater.*, 144 (2007) 355–362.
- [4] A. Kurniawan, H. Sutiono, N. Indraswati, S. Ismadi, Removal of basic dyes in binary system by adsorption using rarasaponin-bentonite: Revisited of extended Langmuir model, *Chem. Eng. J.*, 189–190 (2012) 264–274.
- [5] P. Pradhan, G. Babu, Biological decolonization of Reactive Red 31 and Reactive Yellow 81 dyes by novel isolated bacterial strain *Streptococcus* sp. VBH1, *Int. J. Curr. Res.*, 4 (2012) 10–16.
- [6] S.S. Moghaddam, M.R. Moghaddam, M. Arami, Coagulation/flocculation process for dye removal using sludge from water treatment plant: optimization through response surface methodology, *J. Hazard. Mater.*, 175 (2010) 651–657.
- [7] X. Chen, Y. Zhao, J. Moutinho, J. Shao, A.L. Zydney, Y. He, Recovery of small dye molecules from aqueous solutions using charged ultra filtration membranes, *J. Hazard. Mater.*, 284 (2015) 58–64.
- [8] A. Ikhlaq, D.R. Brown, B. Kasprzyk-Hordern, Catalytic ozonation for the removal of organic contaminants in water on alumina, *Appl. Catal. B-Environ.*, 165 (2015) 408–418.
- [9] M. Kousha, E. Daneshvar, M.S. Sohrabi, M. Jokar, A. Bhatnagar, Adsorption of acid orange II dye by raw and chemically modified brown macroalga *Stoechospermum marginatum*, *Chem. Eng. J.*, 192 (2012) 67–76.
- [10] L. Cottet, C.A.P. Almeida, N. Naidek, M.F. Viante, M.C. Lopes, N.A. Debacher, Adsorption characteristics of montmorillonite clay modified with iron oxide with respect to methylene blue in aqueous media, *Appl. Clay Sci.*, 95 (2014) 25–31.
- [11] P. Sivakumar, P.N. Palanisamy, Adsorption studies of basic red 29 by a non-conventional activated carbon prepared from *Euphorbia antiquorum* L, *Int. J. Chem. Tech. Res.*, 1 (2009) 502–510.
- [12] R. Elmoubarki, F.Z. Mahjoubi, H. Tounsadi, J. Moustadraf, M. Abdennouri, A. Zouhri, A. El Albani, N. Barka, Adsorption

- of textile dyes on raw and decanted moroccan clays: Kinetics, equilibrium and thermodynamics, *Water Resour. Ind.*, 9 (2015) 16–29.
- [13] S. Lin, Z. Song, G. Che, A. Ren, P. Li, C. Liu, J. Zhang, Adsorption behavior of metal–organic frameworks for methylene blue from aqueous solution, *Micropor. Mesopor. Mater.*, 193 (2014) 27–34.
- [14] E. Errais, J. Duplay, F. Darragi, I. M'Rabet, A. Aubert, F. Huber, G. Morvan, Efficient anionic dye adsorption on natural untreated clay: Kinetic study and thermodynamic parameters, *Desalination*, 275 (2011) 74–81.
- [15] M. Kırınşan, R.D.C. Soltani, A. Hassani, S. Karaca, A. Khataee, Preparation of cetyltrimethylammonium bromide modified montmorillonite nanomaterial for adsorption of a textile dye, *J. Taiwan Inst. Chem. Eng.*, 45 (2014) 2565–2577.
- [16] J.L. Chang, J.C. Ma, Q.L. Ma, D.D. Zhang, N.N. Qiao, M.X. Hu, H.Z. Ma, Adsorption of methylene blue onto Fe₃O₄/activated montmorillonite nanocomposite, *Appl. Clay Sci.*, 119 (2016) 132–140.
- [17] A. Middea, L.S. Spinelli, F.G. Souza, R. Neumann, T.L.A.P. Fernandes, O.D.M. Gomes, Preparation and characterization of an organo-palygorskite-Fe₃O₄ nanomaterial for removal of anionic dyes from wastewater, *Appl. Clay Sci.*, 139 (2017) 45–53.
- [18] A. Czimerova, J. Bujdak, R. Dohrmann, Traditional and novel methods for estimating the layer charge of smectites, *Appl. Clay Sci.*, 34 (2006) 2–13.
- [19] M. Madeira, E. Auxtero, E. Sousa, Cation and anion exchange properties of andisols from the Azores, Portugal, as determined by the compulsive exchange and the ammonium acetate methods, *Geoderma*, 117 (2003) 225–241.
- [20] J.F. Liu, Z.S. Zhao, G.B. Jiang, Coating Fe₃O₄ magnetic nanoparticles with humic acid for high efficient removal of heavy metals in water, *Environ. Sci. Technol.*, 42 (2008) 6949–6954.
- [21] X.C. Ma, F. Xu, L.Y. Chen, Z.D. Zhang, Y. Du, Y. Xie, Magnetic fluids for synthesis of the stable adduct T-Fe₂O₃/CTAB/Clay, *J. Cryst. Growth*, 280 (2005) 118–125.
- [22] Y. Bessekhoud, D. Robert, J.V. Weber, N. Chaoui, Effect of alkaline-doped TiO₂ on photo catalytic efficiency, *J. Photochem. Photobiol. A: Chem.*, 167 (2004) 49–57.
- [23] Z.J. Zhang, X.Y. Chen, B.N. Wang, C.W. Shi, Hydrothermal synthesis and self-assembly of magnetite (Fe₃O₄) nanoparticles with the magnetic and electrochemical properties, *J. Cryst. Growth*, 310 (2008) 5453–5457.
- [24] L. Zhang, Z. Wu, L.W. Chen, L.J. Zhang, X.L. Li, H.F. Xu, H.Y. Wang, G. Zhu, Preparation of magnetic Fe₃O₄/TiO₂/Ag composite micro spheres with enhanced photo catalytic activity, *Solid State Sci.*, 52 (2016) 42–48.
- [25] H. Aghdasinia, A. Khataee, M. Sheikhi, P. Takhtfiroozeh, Pilot plant fluidized-bed reactor for degradation of basic blue 3 in heterogeneous Fenton process in the presence of natural magnetite, *Environ. Prog. Sustain. Energy*, 36 (2017) 1039–1048.
- [26] Ö. Açışlı, S. Karaca, A. Gürses, Investigation of the alkyl chain lengths of surfactants on their adsorption by montmorillonite (Mt) from aqueous solutions, *Appl. Clay Sci.*, 142 (2017) 90–99.
- [27] S.M. Lee, D. Tiwari, Organo and inorgano-organo-modified clays in the remediation of aqueous solutions: An overview, *Appl. Clay Sci.*, 59–60 (2012) 84–102.
- [28] L.M. Wu, C.H. Zhou, D.S. Tong, W.H. Yu, H. Wang, Novel hydrothermal carbonization of cellulose catalyzed by montmorillonite to produce kerogen-like hydrochar, *Cellulose*, 21 (2014) 2845–2857.
- [29] O. Acisli, A. Khataee, S. Karaca, M. Sheydaei, Modification of nanosized natural montmorillonite for ultrasound-enhanced adsorption of Acid Red 17, *Ultrason. Sonochem.*, 31 (2016) 116–21.
- [30] M. Hajjaji, H. El Arfaoui, Adsorption of methylene blue and zinc ions on raw and acid-activated bentonite from Morocco, *Appl. Clay Sci.*, 46 (2009) 418–421.
- [31] G. Magnacca, A. Allera, E. Montoneri, L. Celi, D.E. Benito, L.G. Gagliardi, M.C. Gonzalez, D.O. Martire, L. Carlos, Novel magnetite nanoparticles coated with waste-sourced biobased substances as sustainable and renewable adsorbing materials, *ACS Sustain. Chem. Eng.*, 2 (2014) 1518–1524.
- [32] M. Toor, B. Jin, Adsorption characteristics, isotherm, kinetics, and diffusion of modified natural bentonite for removing diazo dye, *Chem. Eng. J.*, 187 (2012) 79–88.
- [33] A. Hassani, F. Vafaei, S. Karaca, A.R. Khataee, Adsorption of a cationic dye from aqueous solution using Turkish lignite: Kinetic, isotherm, thermodynamic studies and neural network modeling, *J. Ind. Eng. Chem.*, 20 (2014) 2615–2624.
- [34] M.T. Yagub, T.K. Sen, H.M. Ang, Equilibrium, kinetics, and thermodynamics of methylene blue adsorption by pine tree leaves, *Water Air Soil Pollut.*, 223 (2012) 5267–5282.
- [35] E.N. El Qada, S.J. Allen, G.M. Walker, Adsorption of methylene blue onto activated carbon produced from steam activated bituminous coal: A study of equilibrium adsorption isotherm, *Chem. Eng. J.*, 124 (2006) 103–110.
- [36] S. Karaca, A. Gürses, M. Acikyildiz, M. Ejder, Adsorption of cationic dye from aqueous solutions by activated carbon, *Micropor. Mesopor. Mater.*, 115 (2008) 376–382.
- [37] M.M.F. Silva, M.M. Oliveira, M.C. Avelino, M.G. Fonseca, R.K.S. Almeida, E.C. Silva, Adsorption of an industrial anionic dye by modified-KSF-montmorillonite: Evaluation of the kinetic, thermodynamic and equilibrium data, *Chem. Eng. J.*, 203 (2012) 259–268.
- [38] M. Mana, M.S. Ouali, L.C. de Menoryal, J.J. Zajac, C. Charnay, Regeneration of spent bleaching earth by treatment with cetyltrimethylammonium bromide for application in elimination of acid dye, *Chem. Eng. J.*, 174 (2011) 275–280.
- [39] Y.S. Ho, G. McKay, Pseudo-second order model for sorption processes, *Process Biochem.*, 34 (1999) 451–465.
- [40] S. Lagergren, About the theory of so called adsorption of soluble substances. *K. Svenska Vetenskapsakad., Handlingar.*, 24 (1898) 1–39.
- [41] W.J. Weber, J.C. Morris, Kinetics of adsorption on carbon from solution, *J. Sanitary Eng. Div.*, 89 (1963) 31–60.
- [42] V. Basavarao, S. Rammohanrao, Adsorption studies on treatment of textile dyeing industrial effluent by flyash, *Chem. Eng. J.*, 116 (2006) 77–84.
- [43] Y. Bulut, H. Aydin, A kinetics and thermodynamics study of methylene blue adsorption on wheat shells, *Desalination*, 194 (2006) 259–267.
- [44] D. Kavitha, C. Namasivayam, Experimental and kinetic studies on methylene blue adsorption by coir pith carbon, *Bioreour. Technol.*, 98 (2007) 14–21.
- [45] A. Gürses, A. Hassani, M. Kiransan, O. Acisli, S. Karaca, Removal of methylene blue from aqueous solution using by untreated lignite as potential low-cost adsorbent: Kinetic, thermodynamic and equilibrium approach, *J. Water Process Eng.*, 2 (2014) 10–21.
- [46] M. Dogan, Y. Ozdemir, M. Alkan, Adsorption kinetics and mechanism of cationic methyl violet and methylene blue dyes onto sepiolite, *Dyes Pigments*, 75 (2007) 701–713.
- [47] L. Eskandarian, M. Arami, E. Pajootan, Evaluation of adsorption characteristics of multiwalled carbon nanotubes modified by a poly(propylene imine) dendrimer in single and multiple dye solutions: Isotherms, Kinetics, and Thermodynamics, *J. Chem. Eng. Data*, 59 (2014) 444–454.
- [48] P.V. Temkin M.J., Recent modifications to Langmuir isotherms, *Acta Phys.-Chim. Sinica.*, 12 (1940) 217–222 (URSS).
- [49] M.U.C. Aharoni, Kinetics of activated chemisorption. Part 2. Theoretical models, *J. Chem. Soc. Faraday Trans.*, 73 (1977) 456–464.